

Elucidating the Effect of Iron Speciation ($\text{Fe}^{2+}/\text{Fe}^{3+}$) on Crystallization Kinetics of Sodium Aluminosilicate Glasses

Yaqoot Shaharyar,[‡] Justin Y. Cheng,[‡] Edmund Han,[‡] Allyson Maron,[‡] Jamie Weaver,[§] José Marcial,[¶] John S. McCloy,[¶] and Ashutosh Goel^{‡,†}

[‡]Department of Materials Science and Engineering, Rutgers-The State University of New Jersey, Piscataway, New Jersey

[§]Department of Chemistry, Washington State University, Pullman, Washington

[¶]School of Mechanical & Materials Engineering and Materials Science & Engineering Program, Washington State University, Pullman, Washington

We report on the influence of Fe_2O_3 on the crystallization kinetics of nepheline ($\text{Na}_2\text{O}\cdot\text{Al}_2\text{O}_3\cdot 2\text{SiO}_2$)-based sodium aluminosilicate glasses. A series of glasses with varying $\text{Al}_2\text{O}_3/\text{Fe}_2\text{O}_3$ content were synthesized in the system $25\text{Na}_2\text{O}-(25-x)\text{Al}_2\text{O}_3-x\text{Fe}_2\text{O}_3-50\text{SiO}_2$ (x varies between 0 and 5 mol%) through melt-quench technique. A systematic set of experiments were performed to elucidate the influence of iron speciation ($\text{Fe}^{2+}/\text{Fe}^{3+}$) on the crystallization kinetics of these glasses including: (1) obtaining the details of nonisothermal crystallization kinetics by differential scanning calorimetry, (2) determining the influence of heat treatment on the structure and iron coordination in glasses by X-ray photoelectron spectroscopy and wet chemistry, and (3) following the crystalline phase evolution in glasses in air and inert environments by X-ray diffraction and scanning electron microscopy. The crystallization of two polymorphs of NaAlSiO_4 —carnegieite (orthorhombic) and nepheline (hexagonal)—was observed in all the glasses, wherein the incorporation of iron promotes the formation of nepheline over carnegieite while shifting the crystallization mechanism from surface to volume. The influence of environment (air versus inert) and iron content on the crystallization kinetics of these glasses is contextualized from the perspective of the devitrification problem usually observed in sodium- and alumina-rich high level nuclear waste glasses.

Keywords: iron-containing glass; nepheline; crystallization kinetics

I. Introduction

UNDERSTANDING the influence of iron on the nucleation and crystallization kinetics of silicate glasses has been of great interest for scientific community. From the geological and industrial standpoint, iron is one of the most important transition-metal elements as it can coexist with the ferric (Fe^{2+}) and ferrous (Fe^{3+}) states in silicate melts. The latter two valences affect melt structure and properties in a specific and often complex way because their relative abundances vary with temperature, pressure, and chemical composition, with strong dependence on oxygen fugacity.^{1–3} Despite their importance and abundance, however, our knowledge of the structural behavior of iron oxides and its implications on various thermodynamic properties is less complete than for

other major components in silicate melts and glasses such as Al_2O_3 .

Iron oxides are integral components of sodium- and aluminum-rich high level radioactive waste liquids stored in steel tanks at the Hanford site in Washington State, USA. Generally, high level waste (HLW) glasses contain Fe_2O_3 in the range of 2–10 wt% with its mean concentration at ~7 wt%.⁴ According to the current strategy, the radioactive waste will be blended with glass-forming chemicals, poured as a slurry, melted at 1150°C, then poured into canisters where the melt solidifies into a vitrified borosilicate glass. The overarching goal of the project is to develop chemically durable glassy waste forms with maximum waste loading in order to minimize cost and maximize long-term environmental stability. However, in the presence of glass-forming SiO_2 and B_2O_3 , a melt rich in Na_2O , Al_2O_3 , and Fe_2O_3 is prone to crystallization of nepheline (NaAlSiO_4)^{5,6} and iron-containing spinel (for example, NiFe_2O_4 , but may contain Mn, Cr, and other minor transition metals).^{7–9} While volume nucleation of NiFe_2O_4 spinel crystals in the melt pool during routine operation of glass melters is problematic, because large insoluble crystals can settle to the floor of the melter and partially or completely block the pour spout,^{7,10} the crystallization of nepheline and related aluminosilicate phases in glass melt during canister cooling can result in severe deterioration of the chemical durability of the final waste form.^{6,11–15} Therefore, it becomes imperative to understand the thermal stability and crystallization kinetics of these multicomponent glasses. However, their compositional complexity (~15 oxide components) does not easily allow for the creation of an all-encompassing dataset for designing glasses with high waste loading and minimal tendency toward nepheline crystallization.^{11,16}

As the HLW borosilicate glasses are similar in composition to basalt or feldspathoid glass on a borate-free basis, and as no borate phases crystallize on the liquidus, the crystallization chemistry of waste glasses can be described by the known phase relations of the geochemical basalt quaternary $\text{Na}_2\text{O}-\text{Al}_2\text{O}_3-\text{Fe}_2\text{O}_3-\text{SiO}_2$ system.^{7,8,17} Accordingly, this study is focused on understanding the influence of structural speciation of iron on the crystallization kinetics of model $\text{Na}_2\text{O}-\text{Al}_2\text{O}_3-\text{Fe}_2\text{O}_3-\text{SiO}_2$ glasses with nepheline-like stoichiometries, $\text{NaFe}_x\text{Al}_{1-x}\text{SiO}_4$ with Fe_2O_3 concentrations in the range of that expected for nuclear waste glasses.

II. Experimental Procedure

(1) Synthesis of the Glasses

A series of glasses with compositions $25\text{Na}_2\text{O}-(25-x)\text{Al}_2\text{O}_3-x\text{Fe}_2\text{O}_3-50\text{SiO}_2$ (mol%), where x varies between 0 and 5, has been prepared by the melt-quenching technique. The glasses have been labeled in accordance with their respective Fe_2O_3

L. Pinckney—contributing editor

Manuscript No. 37739. Received November 4, 2015; approved March 7, 2016.

[†]Author to whom correspondence should be addressed. e-mail: ashutosh.goel@rutgers.edu

content, i.e., Fe-0, Fe-2.5, and Fe-5. The high-purity powders of SiO₂ (Alfa Aesar, Ward Hill, MA; >99.5%), Na₂CO₃ (Sigma Aldrich, St. Louis, MO; >99%), Al₂O₃ (Sigma Aldrich; ≥98%), and Fe₂O₃ (Sigma Aldrich; ≥99%) were used. Homogeneous mixtures of batches (~25 g), obtained by ball milling, were melted in Pt–Rh crucibles at 1650°C for 2 h in air. The glasses were obtained in frit form by quenching the crucible in cold water. The amorphous nature of glasses was confirmed by X-ray diffraction (XRD) analysis (PANalytical B.V., Westborough, MA; X'Pert Pro; CuK_α radiation; 2θ range: 10°–90°; step size: 0.007° s⁻¹). X-ray fluorescence analyzer (Epsilon 1, PANalytical B.V.) equipped with Ag anode X-ray tube was used for the chemical analysis of experimental glasses. Table I presents the values of targeted and experimental glass compositions in wt%.

(2) Structural Analysis of Glasses

Influence of iron on the structure of glasses was studied using O1s and Fe2p X-ray photoelectron spectroscopy (XPS; Thermo K-Alpha; Thermo Fisher Scientific, Waltham, MA). The spectra were collected on powdered glass samples mounted on the sample holder using self-adhesive carbon tape. In order to understand the influence of iron redox (Fe²⁺/Fe³⁺) on the crystallization behavior of glasses, XPS O1s and Fe2p spectra were also collected on glasses heated to temperatures just below their respective crystallization temperatures. Heat treatments were performed in a raising hearth furnace at heating rate of 10°C min⁻¹ in accordance with the crystallization temperatures obtained from differential scanning calorimetry (DSC). The glass samples were air quenched as soon as they reached the desired temperatures. This was done to avoid devitrification in glasses which may lead to incorporation of iron in aluminosilicate crystalline phases, thus, leading to incorrect results. XPS data was collected on quenched samples at room temperature. The outgassing problem was avoided by holding the samples in venting chamber for 60 min before loading them into the X-ray gun chamber.

(3) Fe²⁺/Fe³⁺ Ratio in Glasses by UV-Vis Experiments

A spectrophotometric method using chemically dissolved glass was used to obtain iron redox distribution as follows. A quantity of 0.100 mg of glass powder (mean particle size: ~150 μm) was weighed into a 100 mL Teflon beaker, and ca. 0.50 mL of H₂SO₄ (Sigma Aldrich) and ca. 1.00 mL 48–51% HF (Sigma Aldrich) were added. The mixture was carefully swirled until all particles dissolved into solution. The cooled solution was then diluted to 100.0 mL with deionized distilled water (DDIW) and well mixed. Using a calibrated pipette, 2.0 mL of the solution was transferred to another 100 mL Teflon beaker, and mixed with an addition of 25 mL of DDIW. An ammonium acetate buffer solution was used to adjust the pH of the solution to 3.4 ± 0.01. Then, 5.00 mL of 1, 10 phenanthroline solution was added to the beaker, and the solution was diluted to 50 mL with DDIW.

A Cary 5000 (Agilent, Santa Clara, CA) UV–Vis NIR Spectrophotometry was utilized in this study, and absorption data was obtained with the Cary WinUV software. All samples were measured in transmission mode (%T) at 520 nm in 1 cm plastic cuvettes (3 mL), and referenced to DDIW at ambient temperature (ca. 20°C). Standard solutions contain-

ing known concentrations of Fe as well as glass sample solutions were run in triplicate. A detailed experimental procedure has been published elsewhere.¹⁸

(4) Crystallization Kinetics of Glasses During Heating and Cooling

The glass frit was crushed to obtain coarse glass grains in the particle size range 500 μm–1 mm. All the differential scanning calorimetry (DSC) data was collected using a Simultaneous Thermal Analyzer (STA 8000; Perkin Elmer, Shelton, CT) in the temperature range of 30°C–1580°C. The DSC scans were collected for all the glass samples at heating and cooling rates of 10°C min⁻¹ in air.

In accordance with the crystallization temperatures obtained from DSC data, glasses (5 g frit) were heated (in Al₂O₃ crucibles) to different temperatures at 10°C min⁻¹ and were air quenched as soon as the desired temperatures were reached. Similarly, for understanding the crystalline phase evolution during cooling of glass melt, glass frit was remelted in Pt–Rh crucibles at 1650°C and allowed to cool at β = 10°C min⁻¹. The crucibles were quenched in cold water at various temperatures in accordance with the crystallization data obtained from DTA cooling scans. All the heat treated samples were characterized qualitatively by powder XRD (PANalytical B.V.; X'Pert Pro; CuK_{α1} radiation) and scanning electron microscopy (SEM; ZEISS Sigma, Jena, Germany; FE-SEM).

(5) Understanding the Influence of Environment on Crystallization Kinetics During Heating of Iron-Containing Glasses

In order to understand the influence of environment (air versus inert) on the crystallization kinetics of iron-containing glasses, DSC scans (30°C–1580°C) were collected for glasses Fe-2.5 and Fe-5 at four different heating rates (β = 5, 10, 15, and 20°C min⁻¹) in air and N₂, respectively. The DSC data on glass Fe-0 was collected as reference. The glass grains weighing between 50 and 60 mg were contained in Pt–Rh sample pans while an empty Pt–Rh pan was used as reference. The glass transition temperature (T_g), onset of crystallization (T_c), peak temperature of crystallization (T_p), and melting temperature (T_m) were obtained from these DSC scans. The activation energy of crystallization was calculated using the Augis–Bennett method (Eq. 1),¹⁹ while the Avrami parameter was calculated using Ozawa method (Eq. 2)²⁰

$$\ln\left(\frac{\beta}{T_p}\right) = -\frac{E_c}{RT_p} + \ln k_0 \quad (1)$$

$$\ln[-\ln(1 - \chi)] = -n \ln \beta + \text{constant} \quad (2)$$

where, *R* is the gas constant, *E_c* is the activation energy of crystallization, *χ* is the crystallization fraction obtained from calculating the area under the crystallization curve, *n* is the Avrami parameter, and *k₀* is a constant.

The morphology index (*m*) for all the glasses was calculated using the Kissinger equation modified by Matusita and Sakka (Eq. 3)²¹ and two modifications of the Afify equation (Eqs. 4 and 5) given below:²²

Table I. Chemical Composition of Glasses (wt%)—Batch Versus Experimental

Glass	Batch				Experimental			
	Na ₂ O	Al ₂ O ₃	Fe ₂ O ₃	SiO ₂	Na ₂ O	Al ₂ O ₃	Fe ₂ O ₃	SiO ₂
Fe-0	21.82	35.89	-	42.30	19.99	38.28	-	41.73
Fe-2.5	21.38	31.66	5.51	41.45	19.39	33.45	6.46	40.70
Fe-5	20.96	27.59	10.80	40.64	17.85	29.31	12.98	39.86

$$\ln\left(\frac{T_p^2}{\beta^n}\right) = -\frac{mE_c}{RT_p} + \text{constant} \quad (3)$$

$$\ln\left(\frac{\beta}{T_p^2}\right) = -\frac{mE_c}{nRT_p} + \text{constant} \quad (4)$$

$$\ln(\beta) = -\frac{mE_c}{nRT_p} + \text{constant} \quad (5)$$

The values of m presented in this paper are the averages of the values obtained from the Eqs. 3–5. The values of m obtained by all three methods are within a standard deviation of $\pm 7.5\%$ for each individual glass dataset.

In order to study the influence of heating environment on the crystalline phase evolution in these glasses, all the glasses were heated in the temperature range of 800°C–1000°C for 1 h ($\beta = 10^\circ\text{C min}^{-1}$) in a tube furnace (GSL-1500X-RTP50; MTI Corporation, CA) in air or N_2 (inert) environment. The heat-treated glass samples were allowed to cool to room temperature in the furnace. The quantitative crystalline phase analysis was performed on glass–ceramics obtained after heating the glasses at 900°C for 1 h. The glass-ceramic samples crushed to particle size $< 25 \mu\text{m}$ were analyzed semi-quantitatively by XRD using a Bragg-Brentano diffractometer (PANalyti– X'Pert Pro cal MPD) comprising a Co tube with a Johansson Ge 111 incident beam monochromator for use with $\text{Co } K_{\alpha 1}$ radiation. The quantitative phase analysis of the glass–ceramics was made by the Rietveld method using 10 wt% of corundum Al_2O_3 added as an internal standard. Data were recorded in 2θ range = 5° – 115° (step size 0.02° and 25 s of counting time for each step). The phase fractions were extracted by Rietveld refinements using HighScore Plus (PANalytical B.V.) and were rescaled on the basis of the absolute weight of corundum originally added, and therefore, internally renormalized. Microstructural observations were conducted on fractured glass-ceramic samples (etched by immersion in 2 vol% HF solution for a duration of 2 min) by scanning electron microscopy (SEM; ZEISS Sigma FE-SEM).

III. Results

(1) Glass-Forming Ability

The iron-free parent glass, Fe-0, exhibited good glass-forming ability as amorphous glass was obtained after quenching of the melt in cold water. However, substituting Fe_2O_3 for Al_2O_3 decreased their glass-forming ability and promoted nepheline crystallization ($\text{NaAlSi}_3\text{O}_8$; hexagonal) in the as-quenched glasses. This prompted a decrease in the size of the glass batch from 100 g (oxides) to 25 g in order to increase the quench rate of the glass melt. Although with decreasing batch size, amorphous glasses with 2.5 and 5 mol.% Fe_2O_3 could be obtained; however, incorporation of 7.5 mol.% Fe_2O_3 still resulted in a partially crystallized glass with low carnegite as the crystalline phase as revealed by XRD analysis (not shown). Therefore, glasses with $\text{Fe}_2\text{O}_3 > 5 \text{ mol}\%$ were not synthesized.

(2) Structural Analysis of Glasses

Figure 1 presents Fe2p [Fig. 1(a)] and O1s [Fig. 1(b)] XPS spectra of glasses Fe-2.5 and Fe-5. The peak positions for Fe2p spectra obtained for the iron-containing glasses along with their corresponding $\text{Fe}^{2+}/\text{Fe}^{3+}$ ratios have been presented in Table II, while Table III presents the peak positions and ratios for O1s spectra for all the three glasses. All the spectra were deconvoluted using Gaussian–Lorentzian peak fitting after background subtraction using Shirley's method.²³ The deconvolutions were carried out subject to the

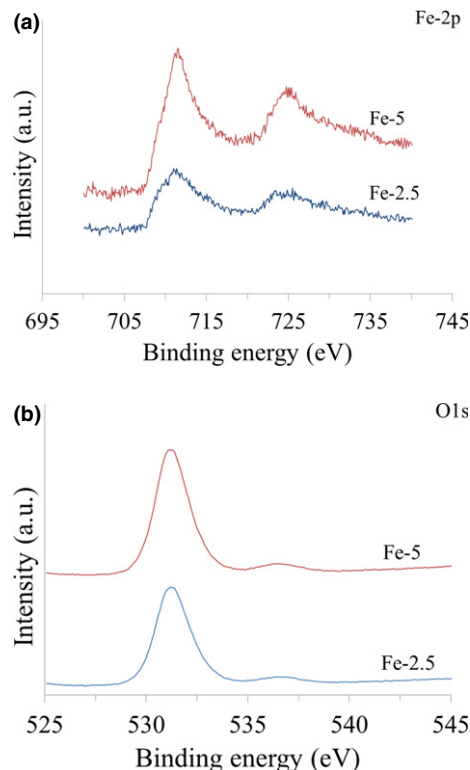


Fig. 1. (a) Fe2p spectra of Fe-2.5 and Fe-5 parent glasses (b) O1s spectra of Fe-2.5 and Fe-5 parent glasses.

constraint of a constant full width half maxima (FWHM) for the same element. According to literature, $\text{Fe}2p_{1/2}$, $\text{Fe}2p_{3/2}$ and the satellite peak positions for Fe^{3+} are located at 724.6, 711.0, and 718.8 eV with standard deviations of 0.17, 0.01, and 0.13, respectively, while for Fe^{2+} the peak positions are located at 722.6, 709.0, and 714.7 eV with standard deviations of 0.05, 0.02, and 0.11, respectively.²⁴ The deconvolution of the Fe2p spectra exhibits a decrease in the $\text{Fe}^{2+}/\text{Fe}^{3+}$ ratio from 0.31 to 0.20 with increasing Fe_2O_3 content from 2.5 to 5 mol.%. The XPS results are in good agreement with those obtained by wet chemistry, where it was observed that $\text{Fe}^{2+}/\text{Fe}^{3+}$ ratio decreases from 0.38 ± 0.07 for glass Fe-2.5 to 0.25 ± 0.09 for glass Fe-5.

The O1s spectra of glasses with $\text{Al}/\text{Na} < 1$ generally comprise three oxygen chemical states, BO1, BO2, and NBO. The BO1 state corresponds to $\text{Si}^{\text{IV}}\text{--O--Si}^{\text{IV}}$ linkage, BO2 corresponds to $\text{Si}^{\text{IV}}\text{--O--Al}^{\text{IV}}$ linkages, and NBO refers to non-bridging oxygens. An alkali aluminosilicate glass with $\text{Al}/\text{Na} = 1$ is considered to be fully polymerized, therefore its O1s XPS only comprises BO1 and BO2 components.^{25–27} Accordingly, an NBO component was not observed in the O1s spectra of parent glass Fe-0. Further in accordance with aluminum avoidance principle, $\text{Al}^{\text{IV}}\text{--O--Al}^{\text{IV}}$ bridges are presumed not to exist in the studied glasses. The partial substitution of Al_2O_3 with Fe_2O_3 leads to depolymerization in glasses as is evident from decreasing $\text{BO1}/\sum\text{BO}$ ratio. Therefore, the presence of NBOs in iron-containing glasses cannot be negated, but their concentration in the studied glasses seems to be significantly low and cannot be detected by O1s spectra¹ as shown in Fig. 2. Therefore, ^{57}Fe Mossbauer spectroscopy and ^{17}O NMR spectroscopy are required to deduce the precise coordination of iron and fraction of NBOs in these glasses, respectively. We are still not sure about the reason for increase in $\text{BO2}/\sum\text{BO}$ ratio. In any case, the $\text{Si}^{\text{IV}}\text{--O--}$

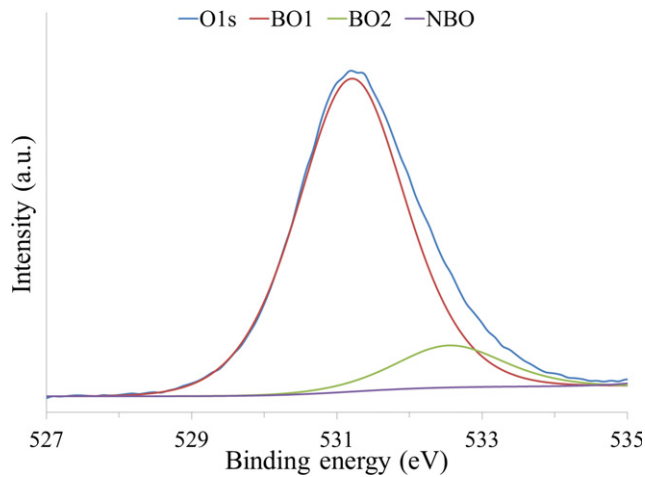
¹NBO peak in O1s spectra is the component with the lowest binding energy. Its intensity decreases in Na–Al–Si–O glasses up to $\text{Al}/\text{Na} = 1$ relative to the scaled intensity of the main “BO peak”. Also, the “BO peak” broadens and shifts to lower binding energy by about 1 eV with increasing Al/Na .

Table II. Peak Positions and Fe²⁺/Fe³⁺ Ratios for Fe2p Spectra Obtained for the Iron-Containing Glasses

	Fe ²⁺		Fe ³⁺		Fe ²⁺ /Fe ³⁺	Fe ²⁺ /Fe	Fe ³⁺ /Fe
	Fe2p _{1/2}	Fe2p _{3/2}	Fe2p _{1/2}	Fe2p _{3/2}			
Fe-2.5							
Parent	722.05	709.02	724.50	711.40	0.31	0.24	0.76
Heat treated	722.08	709.08	724.42	711.35	0.27	0.21	0.79
Fe-5							
Parent	722.00	709.20	724.70	711.60	0.20	0.17	0.83
Heat treated	721.95	709.00	724.65	711.52	0.19	0.16	0.84

Table III. Peak Positions and Ratios for O1s Spectra Obtained for the Iron-Containing Glasses

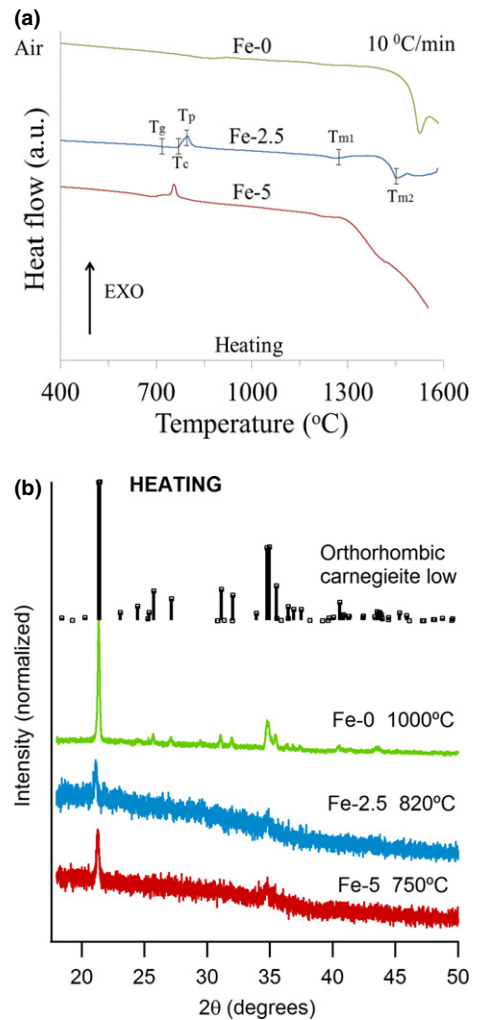
	BO1	BO2	BO1/ΣBO	BO2/ΣBO
Fe-0	532.68	531.25	0.89	0.11
Fe-2.5	532.55	531.20	0.87	0.13
Fe-5	532.16	531.10	0.79	0.21

**Fig. 2.** Deconvoluted O1s XPS spectra of glass Fe-2.5 showing the peak fits for BO1, BO2, NBO.

Al^{IV} and Si^{IV}-O-Fe^{IV} bond linkages corresponding to BO2 will be weaker than Si^{IV}-O-Si^{IV} linkages.

(3) Crystallization Kinetics of Glasses in Air

Figure 3(a) presents the DSC thermographs (in air) of the investigated glasses during heating from 30°C to 1580°C at 10°C min⁻¹, while Table IV presents the values of all the thermal parameters obtained for these glasses. The glass transition temperature (T_g) for glasses Fe-0 and Fe-2.5 has been presented in Table IV, but it was difficult to determine the T_g value for glass Fe-5. The T_g for glasses decreased with partial substitution of Fe₂O₃ for Al₂O₃. With reference to crystallization behavior of glasses, a broad and shallow exothermic hump for glass Fe-0 in the temperature range of 800°C–1000°C was observed, but it was difficult to identify the precise onset (T_c) and peak temperature of crystallization (T_p). The partial substitution of Fe₂O₃ for Al₂O₃ in these glasses not only increased their tendency toward devitrification (as is evident from sharp exothermic crystallization curve) but also shifted the crystallization toward lower temperatures. XRD data of glasses heated (and air quenched) at various temperatures, in accordance with the crystallization temperatures obtained from DSC, reveal that crystallization in all the glasses initiated through the formation of low car-

**Fig. 3.** (a) DSC thermographs (in air) of all the three investigated glasses during heating from 30°C to 1580°C at 10°C min⁻¹; (b) XRD patterns of glasses heated in air to the crystallization temperatures as observed by DSC heating experiments, then air quenched; reference PDF shown is 98-007-3511.

negieite (NaAlSiO₄; orthorhombic) as shown in Fig. 3(b) followed by transformation of carnegieite to nepheline (hexagonal) at higher temperatures. Fe2p XPS spectra of glasses heat treated just below their crystallization temperatures revealed that Fe²⁺/Fe³⁺ ratio for glass Fe-2.5 changed from 0.31 to 0.27 upon heat treatment, while no such change was observed for glass Fe-5 (Fe²⁺/Fe³⁺ = 0.19 after heat treatment) (Table II).

The crystallization in DSC was followed by the appearance of endothermic curves corresponding to melting of crystalline phases in the temperature range of 1245°C–1275°C (T_{m1}) and 1415°C–1530°C (T_{m2}) (Table IV). While only one

Table IV. Thermal Parameters Obtained from DSC During Heating at 10°C min⁻¹

Glass	T_g	T_c	T_p	T_{m1}	T_{m2}
Air					
Fe-0	895	†	†	†	1530
Fe-2.5	718	770	799	1272	1451
Fe-5	†	746	755	1245	1417
N ₂					
Fe-0	895	†	†	†	1530
Fe-2.5	709	768	788	1272	1466
Fe-5	†	746	756	1244	1413

†These parameters could not be reliably determined from the collected DSC data.

All temperature values are in °C.

endothermic melting curve at 1530°C could be observed for glass Fe-0, iron-containing glasses (Fe-2.5 and Fe-5) exhibited two evident melting endotherms indicating the melting of two or more crystalline phases. The melting temperatures were observed to decrease with increasing iron content in glasses.

During cooling of glass melts from 1580°C to 30°C at 10°C min⁻¹, DSC thermographs of all the glasses exhibited two exothermic events—first in the high-temperature region, just below the melting curve, i.e., 1200°C–1500°C, and second in the low temperature region, i.e., 650°C–700°C [Fig. 4(a); Table V]. The appearance of two exothermic curves during cooling suggests formation of two or more crystalline phases. In order to identify these phases, glasses were melted at 1650°C for 1 h and then allowed to cool at 10°C min⁻¹ to the crystallization temperatures (determined from cooling scan of DSC) at which point the crucibles were water quenched. X-ray diffractograms reveal that during cooling of glass melt, crystallization in all the glasses began with the formation of low carnegieite in the 1200°C–1500°C region [Fig. 4(b)]. However, striking differences could be observed in the low temperature region, i.e., 650°C–700°C [Fig. 4(c)] as a function of iron content in glasses. The low carnegieite was still the major crystalline phase in iron-free glass, Fe-0, while iron-containing glasses also crystallized obvious nepheline (NaAlSiO₄; hexagonal). Shannon and Berzins²⁸ reported similar results upon thermal analysis of NaAlSiO₄-based ceramics using differential thermal analysis (DTA), wherein, they observed an exothermic peak on cooling beginning at 690°C and ending at 640°C corresponding to transformation of carnegieite to nepheline. The crystalline microstructure of the glass-ceramics (as observed using SEM) formed during cooling from glass melt to the 1200°C–1500°C region is significantly different from microstructures obtained after cooling to 650°C–700°C (particularly for Fe₂O₃-containing compositions) as is evident from Fig. 5. In correlation with the XRD data, it is assumed that the dominant platelet structures observed in Figs. 5(a) and (b) corresponds to low carnegieite, while the diffuse small crystalline microstructure observed in Fig. 5(a) corresponds to nepheline.

Figure 6(a) presents $\ln(\beta/T_p)$ vs $1/T_p$ plots obtained from the DSC data during heating of glasses Fe-2.5 and Fe-5, in air at different heating rates, which were used to calculate the values for activation energy of crystallization (E_c) listed in Table VI. Similarly, Fig. 6(b) presents representative $\ln[-\ln(1-\chi)]$ vs $\ln \beta$ plots which were used to calculate the Avrami parameter (n) listed in Table VI. The nonisothermal crystallization kinetics of glass Fe-0 could not be studied using DSC, as no well-defined crystallization curve could be obtained from this glass at any heating rate. The activation energy values (in air) showed a significant decrease with increasing Fe₂O₃ content from 2.5 mol.% (~411 kJ mol⁻¹) to 5 mol.% (~295 kJ mol⁻¹) while the Avrami parameter (n) increased from 1.8 (Fe-2.5) to 3.0 (Fe-5) indicating a shift in

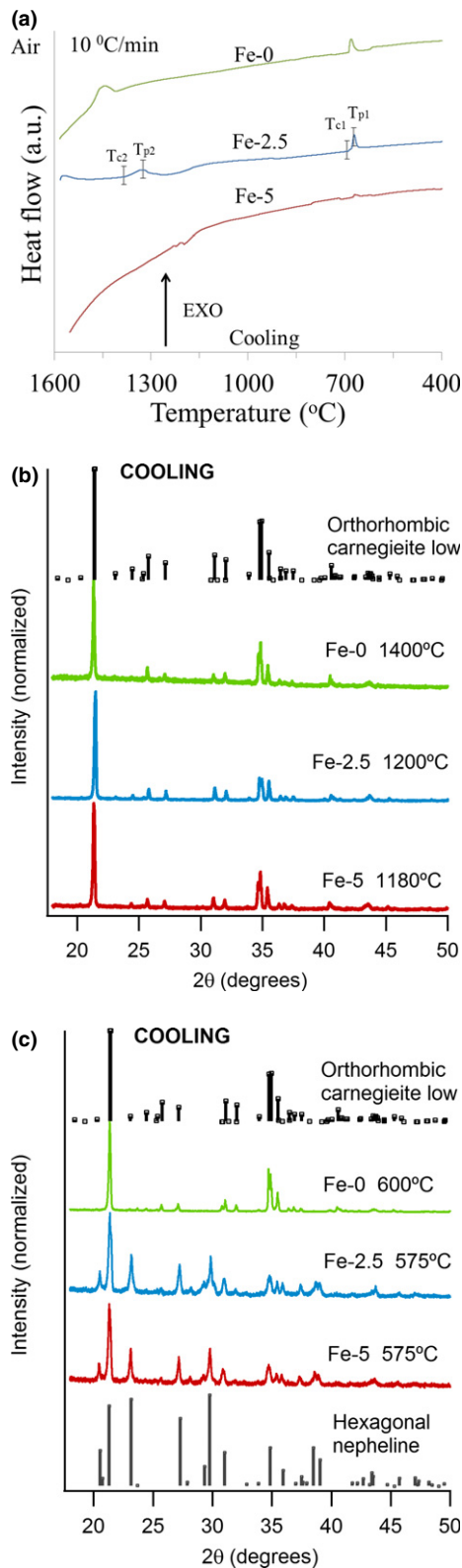


Fig. 4. (a) DSC thermographs of glasses during cooling (in air) at 10°C min⁻¹; (b) XRD patterns of glasses melted at 1650°C for 1 h, then cooled at 10°C min⁻¹ to 1200°C–1400°C (high crystallization temperature as determined by DSC cooling experiments), then water quenched; (c) XRD patterns of glasses melted at 1650°C for 1 h, then cooled at 10°C min⁻¹ to 575°C–600°C (low crystallization temperature as determined by DSC cooling experiments), then water quenched reference PDFs shown are 98-007-3511 for carnegieite and 98-000-0327 for nepheline.

crystallization mechanism of glasses from surface in Fe-0 (as will be shown below) to volume nucleation. The corresponding value of the morphology index (m) also increased from

Table V. Thermal Parameters Obtained from DSC During Cooling at 10°C min⁻¹

Glass	T_{c1}	T_{p1}	T_{c2}	T_{p2}
Air				
Fe-0	1483	1466	686	685
Fe-2.5	1332	1304	680	674
Fe-5	†	1230	673	652
N ₂				
Fe-0	1483	1466	686	685
Fe-2.5	†	1219	682	675
Fe-5	1264	1229	672	667

†These parameters could not be reliably determined from the collected DSC data.

All temperature values are in °C.

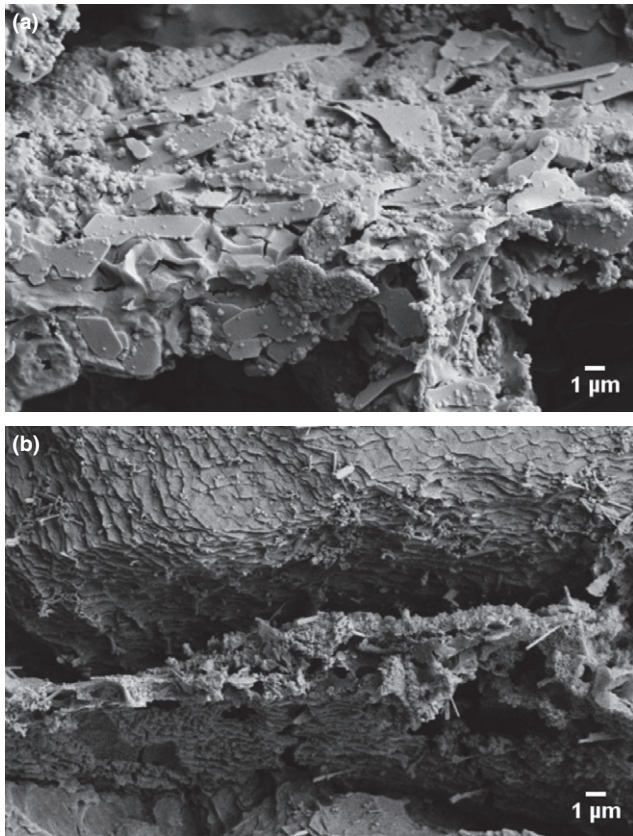


Fig. 5. (a) Crystalline microstructure of Fe-5 glass melt cooled to 1180°C and water quenched; (b) Crystalline microstructure of Fe-5 glass melt cooled to 575°C and water quenched.

1.81 (Fe-2.5) to 2.90 (Fe-5) (Table VI). It should be noted that for $n = m$, it implies that the glasses were prenucleated and no nucleation occurred during thermal treatment.^{29,30} As per the DSC data, the crystallization in glass Fe-2.5 occurs predominantly *via* two-dimensional disk-like growth ($n = m = \sim 2$) while, in glass Fe-5, the values of the parameters n and m suggest spherical three-dimensional growth of crystals ($n = m = \sim 3$).³⁰

Figure 7(a) presents the XRD data of powdered glass-ceramics obtained by heat treatment of glasses at 900°C for 1 h, while Fig. 7(b) presents the quantitative phase analysis of these glass-ceramics as obtained by Rietveld method. As mentioned above, low carnegieite is the preferred crystalline phase in the iron-free glass-ceramic composition, while nepheline crystallized in minor quantities. However, incorporating Fe₂O₃ in the glasses not only increased their overall crystallization tendency (lower amorphous fraction) but also

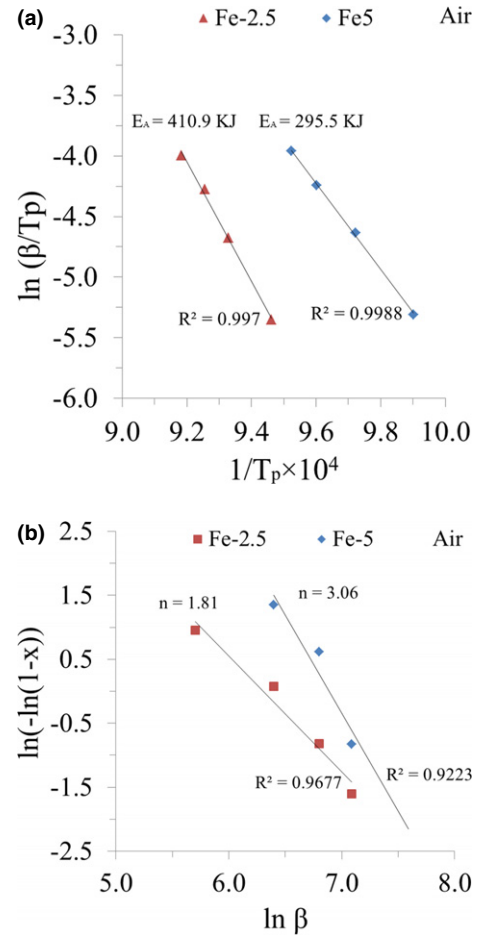


Fig. 6. (a) Activation energy of crystallization for glasses Fe-2.5 and Fe-5 in air calculated using Eq. 1; (b) Avrami parameter of glasses Fe-2.5 and Fe-5 in air calculated using Eq. 2.

Table VI. Activation Energies (E_c), Avrami Parameter (n), and Morphology Index (m) of Glasses Fe-0, Fe-2.5, and Fe-5

Sample	Environment	Activation energy (kJ/mole)	Avrami (n)	Average Morphology index (m)
Fe-2.5	Air	410.89	1.81	1.81
Fe-2.5	N ₂	372.18	1.95	1.87
Fe-5	Air	295.47	3.06	2.90
Fe-5	N ₂	302.88	3.11	3.13

led to a sharp increase in the propensity of nepheline formation at the expense of carnegieite. Furthermore, trace amount of magnetite (Fe₃O₄) was observed in glass-ceramic Fe-5 which possibly acted as a nucleation site in the studied glass compositions. The SEM image of glass Fe-0 crystallized at 900°C for 1 h [Fig. 8(a)] depicts the growth of platelike crystals from the edges of the glass toward the interior, thus confirming the dominance of surface crystallization in iron-free glass (Fe-0). No evidence of surface crystallization was observed in iron-containing glass Fe-5 after heat treatment at 900°C for 1 h as is evident from Fig. 8(b).

(4) Crystallization Kinetics of Glasses in Inert Environment

The DSC thermographs of all the investigated glasses, when heated in an inert environment (N₂) from 30°C to 1580°C at 10°C min⁻¹, have been presented in Fig. 9, while the thermal parameters obtained have been summarized in Table IV. As

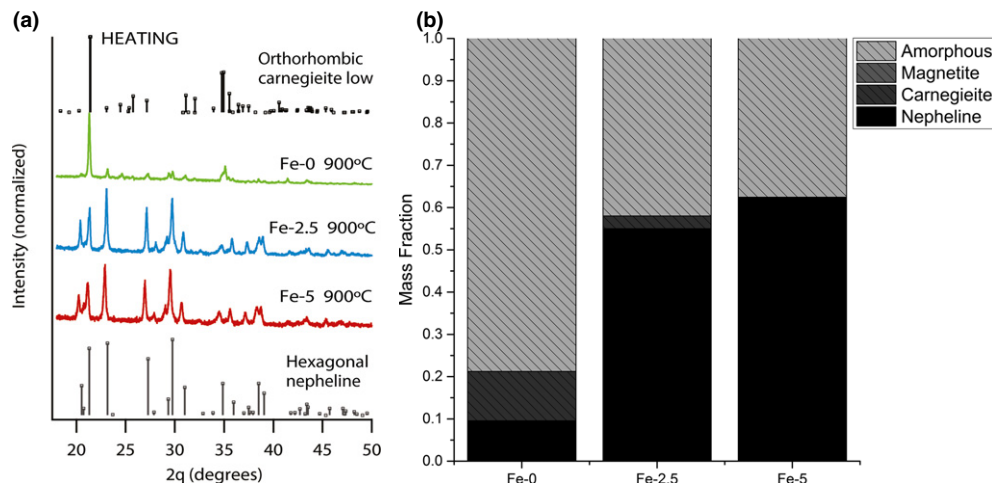


Fig. 7. (a) Qualitative crystalline phase analysis by XRD; and (b) quantitative crystalline phase analysis (by Rietveld—RIR analysis) of glass-ceramics Fe-0, Fe-2.5, and Fe-5 obtained after heat treatment of parent glasses at 900°C for 1 h in air.

was the case with the DSC thermographs in air, T_g could not be observed in DSC scans of glasses Fe-0 and Fe-5. With reference to crystallization behavior of Fe-0 in DSC, we again observed a broad, exothermic hump in the temperature range of 800°C–1000°C and it was difficult to identify the precise onset (T_c) and peak temperature of crystallization (T_p). The T_g for glass Fe-2.5 was observed at 709°C which is $\sim 10^\circ\text{C}$ lower than that observed for this glass in air. Also, the crystallization temperatures for glass Fe-2.5 ($T_c = 768^\circ\text{C}$ and $T_p = 788^\circ\text{C}$) were observed to be slightly lower than their corresponding values in air. However, all the crystallization and melting temperatures for glass Fe-5 heated in inert environment ($T_c = 768^\circ\text{C}$, $T_p = 788^\circ\text{C}$, $T_{m2} = 1413^\circ\text{C}$) were similar to those obtained for this glass in air.

Figure 10(a) presents the $\ln(\beta/T_p)$ vs $1/T_p$ plots for glasses Fe-2.5 and Fe-5 (in inert environment) while the values of activation energy of crystallization (E_c) are presented in Table VI. The activation energy values (in N_2) showed a significant decrease with increasing Fe_2O_3 content in glasses from 2.5 mol.% ($\sim 372 \text{ kJ mol}^{-1}$) to 5 mol.% ($\sim 303 \text{ kJ mol}^{-1}$). When compared with the crystallization kinetics data obtained from thermal analysis of glasses in air, the E_c values for glass Fe-2.5 heated in nitrogen are significantly lower (411 kJ mol^{-1} in air vs 372 kJ mol^{-1} in N_2), whereas E_c for glass Fe-5 is very similar in both the environments (295 kJ mol^{-1} in air vs 303 kJ mol^{-1} in N_2). The values of the Avrami parameter (n) [Fig. 10(b); Table VI] increased from 1.95 (Fe-2.5) to 3.11 (Fe-5), indicating a shift in crystallization mechanism of glasses from surface [for glass Fe-0 as shown in Fig. 8(a)] to volume nucleation. Further, $n \approx m$ for iron-containing glasses suggest that glasses are prenucleated.

The crystallization kinetics data obtained from DSC is well supported by the crystalline phase evolution in glasses when heated at 900°C for 1 h in N_2 environment. At a qualitative level, there was no significant influence of environment (air versus inert) on the crystalline phase evolution in the investigated glasses, as carnegieite was still a favored phase in glass Fe-0 while iron incorporation promoted the crystallization of nepheline. The quantitative phase analysis (Fig. 11) corroborated the results from qualitative phase analysis.

IV. Discussion

(1) Structural Role of Iron in Glasses

In a meta-aluminosilicate glass, charge compensation of Al^{3+} in tetrahedral coordination is accomplished with either alkali or alkaline-earth cations. Ideally, a meta-aluminosili-

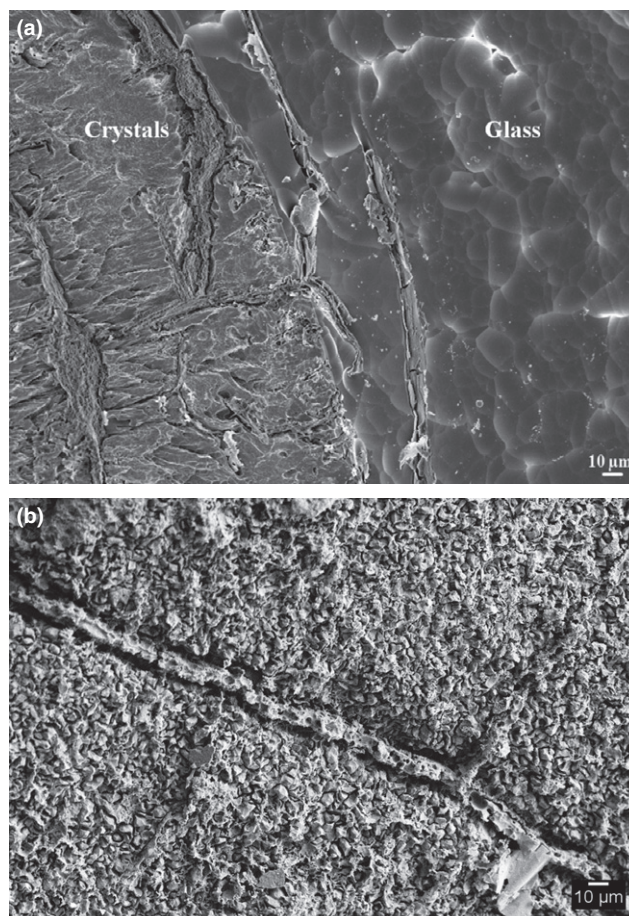


Fig. 8. (a) Secondary electron (SE) image of glass Fe-0 crystallized at 900°C for 1 h; (b) SE image of glass Fe-5 after heat treatment at 900°C for 1 h.

cate glass is considered to be fully polymerized. While this hypothesis is valid for alkali aluminosilicate glasses (for example, Fe-0), nonbridging oxygens (NBOs) have been shown to exist in the structure of alkaline-earth meta-aluminosilicate glasses.^{31,32} Further literature reveals that there exists a considerable structural resemblance between glasses along the SiO_2 – NaAlO_2 and pure SiO_2 as only subtle structural variations with $\text{Al}/(\text{Al}+\text{Si})$ can be observed,

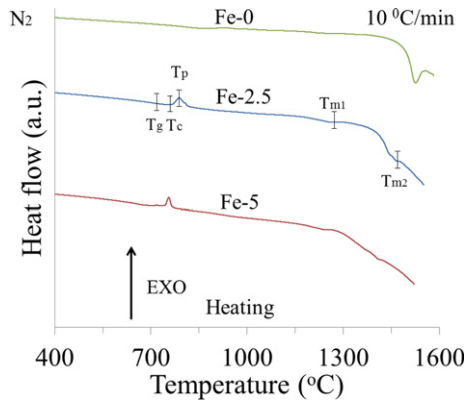


Fig. 9. DSC thermographs (in N₂) during heating from 30°C to 1580°C at 10°C min⁻¹.

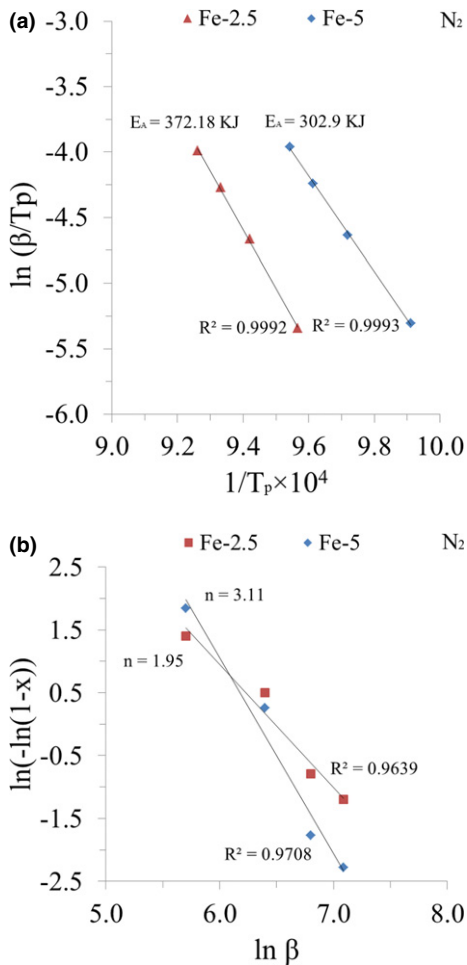


Fig. 10. (a) Activation energy of crystallization for glasses Fe-2.5 and Fe-5 in N₂ calculated using Eq. 1; (b) Avrami Parameter for glasses Fe-2.5 and Fe-5 in N₂ calculated using Eq. 2.

pointing to a simple network structure smoothly varying between pure SiO₂ to at least NaAlSiO₄ composition (Fe-0 in this case).³³ Therefore, any presence of NBOs in this system is highly unlikely as has also been shown by O1s XPS spectra of glass Fe-0.

When iron oxide is incorporated into a glass melt, the relative proportions of Fe²⁺ and Fe³⁺ may depend on several factors including chemical composition of the melt, total iron content, oxygen fugacity, and temperature. For any melt, the temperature dependence of redox reaction causes Fe²⁺/Fe³⁺ to be the lowest near the glass transition and the highest at superliquidus temperatures. The changes in the relative abun-

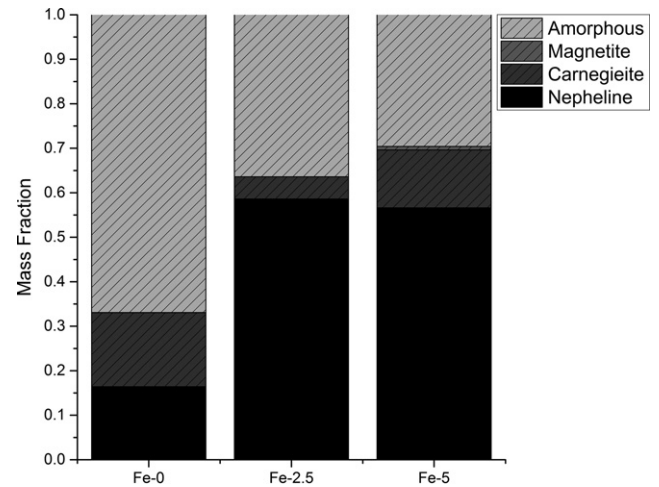


Fig. 11. Quantitative phase analysis of Fe-0, Fe-2.5, and Fe-5 glass-ceramics in N₂ as obtained by Rietveld-RIR method.

dances of ferrous and ferric ions are simply described by the reaction: $2\text{FeO} + \frac{1}{2} \text{O}_2 \leftrightarrow \text{Fe}_2\text{O}_3$. At constant temperature and pressure, the equilibrium constant of this reaction depends on the activities of FeO and Fe₂O₃ in the melt, which are both complex functions of composition, and especially of oxygen fugacity. In the present case, considering that temperature and oxygen fugacity are constant, the decrease in Fe²⁺/Fe³⁺ ratio with increasing Fe₂O₃ content from 2.5 mol.% to 5 mol.% in glasses may be attributed to the chemical effect. Similar observations were reported in FeO-SiO₂ binary system wherein an increase in Fe³⁺/ΣFe was observed with increasing iron content and was explained on the basis of a purely chemical effect; everything being equal, the opposite variation would be produced by the concomitant rise of liquidus temperatures.³³

In this study, the structural analysis of glasses by XPS reveals that iron incorporation results in depolymerization of the aluminosilicate glass network possibly by creating NBOs. These results are also substantiated by decrease in glass transition (*T_g*) and melting temperature (*T_m*) with increasing Fe₂O₃ content. According to Richet and Bottinga,³⁴ the compositional dependence of *T_g* of sodium aluminosilicate glasses is so strong that minor deviations from nominal Na/(Na+Al) stoichiometry can spread *T_g* over of a hundred degrees. Iron oxide is known to act as an intermediate in oxide glasses, its structural role being dictated by Fe²⁺/Fe³⁺ ratio and the way Fe³⁺ reacts with oxygen in the glass melt. As a network former, Fe³⁺ is likely coordinated tetrahedrally with oxygen (Fe₂O₃ + O²⁻ ↔ 2 FeO₂⁻). In contrast to its SiO₂ counterpart, FeO₂⁻ bears a negative charge, due to the 3+ valence of iron, which must be compensated by another cation. Similar to Al³⁺ in this role, Fe³⁺ induces polymerization by consuming an oxygen ion. It differs from Al³⁺, however, in that it can also be, on its own, an octahedral network modifier, even when other cations could provide charge compensation for tetrahedral coordination. On the other hand, when produced by the reaction: $\text{Fe}_2\text{O}_3 \leftrightarrow 2 \text{Fe}^{3+} + 3 \text{O}^{2-}$, Fe³⁺ then induces depolymerization of the silicate network with the “free” oxygen that is released. In case of ferrous ion (Fe²⁺), it commonly acts as network modifier in silicate glasses.³³ Considering that a large part of the Fe³⁺ ions in the studied glasses are acting as network former, while a small fraction of Fe³⁺ and majority of the Fe²⁺ ions are network modifier, the incorporation of iron in studied glass samples should generate NBOs but in small concentrations beyond the detection limit of O1s XPS. Further, the drop in *T_g* may also be explained on the basis of lower bond energy of Fe-O (407 kJ mol⁻¹) in comparison with Al-O (501.9 kJ mol⁻¹) and Si-O (799.6 kJ mol⁻¹).³⁵ As a consequence, the three-dimensional structure of glass is weakened resulting in a

lower T_g . It should be noted here that since the ferric ion (Fe^{3+}) has higher charge and a lower ionic radius than that of the ferrous ion (Fe^{2+}), this leads to a larger effective charge (charge per surface area) of the ferric ion. As a consequence of this attraction, the binding energy between Fe^{3+} and O^{2-} should be higher than that between Fe^{2+} and O^{2-} .^{36,37} Therefore, even if we account for the presence of both $\text{Fe}^{2+}\text{-O}$ and $\text{Fe}^{3+}\text{-O}$ bonds in the glass structure, the overall three-dimensional network is bound to be weakened.

(2) Crystallization Mechanism in Glasses

With regard to the mechanism of crystallization in glasses, the dominance of surface crystallization in glass Fe-0 may be explained using the concept of reduced glass transition temperature ($T_{gr} = T_g/T_m$), and temperature of maximum crystal nucleation rates (T_{max}). According to Zanotto,³⁸ glasses (free from any nucleating agent) that crystallize internally have $T_{max} > T_g$, and their T_{gr} varies between 0.54 and 0.57. On the other hand, glasses where surface crystallization is the dominant mechanism (for example, glass Fe-0), $T_{max} < T_g$ and $T_{gr} > 0.58$ (for Fe-0, $T_{gr} = 0.65$). Assuming that Stokes–Einstein–Eyring (SEE) equation holds, and the viscosities of undercooled liquids are governed by the Vogel–Fulcher–Tammann (VFT) equation, it has been demonstrated (by analyzing experimental data) that an increase in T_{gr} results in (1) an increase in the temperature of T_{max} , (2) decrease in the magnitude of maximum nucleation rate, (3) a decrease in the ratio of T_{max}/T_g , and (4) an increase in the nucleation time lag at T_{max} .³⁹ Therefore, volume nucleation cannot occur in reasonable times due to limited (slow) molecular rearrangement and long induction time period.⁴⁰

Incorporation of Fe_2O_3 prenucleates the nepheline-based glass compositions resulting in a low activation energy pathway for heterogeneous crystal growth. This assertion is well supported by high crystallization tendency of iron-containing glass melts, decrease in activation energy of crystallization with increasing Fe_2O_3 content, and the values of Avrami parameter (n) and morphology index (m), wherein, $n = m$ for glasses Fe-2.5 and Fe-5. According to the modified Kissinger and Ozawa equation proposed by Matusita and Sakka,²¹ when $n = m$, crystallization occurs with a constant number of nuclei (i.e., a well-nucleated sample with number of nuclei being independent of the heating rate).^{29,30} The surface crystallization was dominant in iron-free glass, Fe-0, while microstructure of glass–ceramics along with $n \approx 2$ for glass Fe-2.5 implies two-dimensional crystal growth. Similarly, $n \approx 3$ for glass Fe-5 points toward volume crystallization with three-dimensional crystal growth. The shift in mechanism of crystallization from surface to volume with iron incorporation may be attributed to the crystallization of magnetite in glasses upon heating which provides nucleation sites in the studied glass system. The role of Fe_2O_3 as nucleating agent *via* clustering of Fe^{3+} ions resulting in crystallization of magnetite (Fe_3O_4) has been well-established in basaltic and clinopyroxene-based alkali/alkaline-earth aluminosilicate glass systems.⁴¹

The higher activation energy of crystallization of glass Fe-2.5 compared to glass Fe-5 can be explained on the basis of their total Fe_2O_3 content. It has been shown that increasing $\text{Fe}_2\text{O}_3/\text{Al}_2\text{O}_3$ content in aluminosilicate glasses results in considerable decrease in their viscosity, thus, promoting crystallization.^{35,42} This decrease in viscosity may be attributed to structural depolymerization in glasses as discussed above. Further, the lower activation energy value for glass Fe-2.5 crystallized in inert environment versus air may be attributed to their $\text{Fe}^{2+}/\text{Fe}^{3+}$ ratio. Klein et al.⁴² have shown that iron-containing glasses exhibit higher viscosity in oxidizing environment (higher Fe^{3+}) than in reducing environment. The negligible impact of environment (air versus inert) on the crystallization kinetics of glass Fe-5 may be attributed to

the mechanism of crystallization in these glasses and the particle size of glass powder (coarse, 500 μm –1 mm) used in DSC analysis. Since incorporating Fe_2O_3 in the studied glasses shifted their mechanism of crystallization from surface to volume, the impact of environment is visible in glass Fe-2.5 which is still in transition from surface \rightarrow volume crystallization ($n \approx 2$), while we did not observe any impact of environment on glass Fe-5 as the crystallization starts from volume of glass ($n \approx 3$).

(3) Crystalline Phase Evolution in Glasses

The first crystalline phase that appeared in all the glass–ceramics (during heating of glass or cooling of glass melt) was orthorhombic carnegieite. Carnegieite is known to be a metastable phase that appears in glass–ceramics before the crystallization of hexagonal nepheline. However, its crystal structure may vary depending on the mechanism of crystallization in glasses. For example, crystallization in TiO_2 -doped nepheline-based glasses has been shown to proceed through phase separation, thus leading to formation of metastable cubic carnegieite which upon further heat treatment breaks down to form nepheline.⁴³ In natural systems, carnegieite is only metastable and forms nepheline below 1247°C.⁴⁴ According to Onuma et al.,⁴⁵ iron incorporation in nepheline lowers the transformation temperature of carnegieite to nepheline, thus leading to preferential crystallization of nepheline at the expense of carnegieite as observed in this study.

(4) Implications for Nuclear Waste Glasses

Nuclear waste glasses in the USA are almost always silicate based, frequently with large concentrations of both aluminum and sodium, leading to crystallization of nepheline on cooling from the melt,¹⁶ along with some iron-containing spinels such as magnetite (Fe_3O_4) or $(\text{Fe}, \text{Ni}, \text{Mn}, \text{Zn}, \text{Sn})^{\text{II}}(\text{Fe}, \text{Cr})^{\text{III}}_2\text{O}_4$.⁴⁶ In fact, it has been argued that spinel provides the nucleation site for nepheline crystallization in complex nuclear waste glasses.⁴⁷ One parametric study assessing the relative importance of the presence of various oxides on the precipitation of nepheline found that Fe_2O_3 (often in natural nephelines⁶) had roughly an equivalent effect to K_2O (also in natural nepheline) and Li_2O , and was only surpassed by high Na_2O and Al_2O_3 as markers for nepheline precipitation tendency.¹⁴ Interestingly, at very high Fe_2O_3 concentrations (much higher than the range studied here), nepheline formation seems to be suppressed, in favor of spinels¹⁶ or, in the case of simultaneously high SiO_2 and Fe_2O_3 glasses with low Al_2O_3 , pyroxenes like acmite (called aegirine in the pure Na end-member, $\text{NaFeSi}_2\text{O}_6$) are the favored crystalline species.⁸ Thus, the role of iron in nuclear waste glasses is complex. However, from this study, it is clear that the increase in Fe_2O_3 up to 5 mol% in stoichiometric nepheline glasses promotes the crystallization of nepheline over carnegieite (which, incidentally, is only very rarely found in nuclear waste glasses⁴⁸) due to bulk nucleation, possibly on magnetite spinels. From this study, the redox ratio obtained by heating in nitrogen versus air had only a small effect on the crystallization. It is not currently known whether the Fe in this study went into the nepheline structure⁴⁹ or only served as a nucleation site for pure sodic nepheline crystallization. Further study is warranted to assess the presence of Fe in the crystalline phases.

V. Summary and Conclusions

Small fractions of Fe_2O_3 up to $x = 5$ mol% were added to nepheline glass ($\text{Na}_2\text{O}\cdot\text{Al}_2\text{O}_3\cdot 2\text{SiO}_2$), resulting in single phase glasses of composition $25\text{Na}_2\text{O}\cdot(25-x)\text{Al}_2\text{O}_3\cdot x\text{Fe}_2\text{O}_3\cdot 50\text{SiO}_2$. Crystallization experiments were performed on heating of quenched glass and on cooling from the melt, and in both cases orthorhombic carnegieite was the first phase to crystallize.

With increasing Fe₂O₃, kinetics show a preference for bulk versus surface crystallization, and the hexagonal nepheline phase fraction becomes the dominant crystal phase during heating (from glass to glass ceramic) as well as during cooling (from melt to glass ceramic at ~575°C). Crystallization in nitrogen versus air showed that with higher Fe²⁺/Fe³⁺ redox ratio, activation energy for crystallization was lowered, due to lower viscosity at T_g with increasing Fe²⁺ content. Total fraction of crystallized glass was also higher in Fe-containing glasses, though the difference between Fe-2.5 and Fe-5.0 glasses was small. Given the ubiquity of iron in sodium aluminosilicate nuclear waste glasses, and the role played by Fe²⁺/Fe³⁺ in altering the crystallization mechanism in nepheline-based glasses, the importance of iron concentration and redox in glass melts as a function of cooling deserves deeper consideration.

Acknowledgment

This research was supported by the US Department of Energy – Office of River Protection, contract# EM0003207, under the direction of Dr. Albert A. Kruger.

References

- V. Magnien, et al., "Kinetics of Iron Oxidation in Silicate Melts: A Preliminary XANES Study," *Chem. Geol.*, **213**, 253–63 (2004).
- V. Magnien, et al., "Kinetics and Mechanisms of Iron Redox Reactions in Silicate Melts: The Effects of Temperature and Alkali Cations," *Geochim. Cosmochim. Acta*, **72** [8] 2157–68 (2008).
- B. Cochain, et al., "Kinetics and Mechanisms of Iron Redox Reactions in Silicate Glasses and Melts: A XANES Study," *GoldSchmidt Conference Abstracts, Geochim. Cosmochim. Acta*, **72**, A170 (2008).
- C. P. Rodriguez, J. S. McCloy, M. J. Schweiger, J. V. Crum, and A. Wanschell, "Optical Basicity and Nepheline Crystallization in High Alumina Glasses (PNNL-20184)," Pacific Northwest National Laboratory, Richland, WA, 2011.
- A. Goel, et al., "Structural Analysis of Some Sodium and Alumina Rich High-Level Nuclear Waste Glasses," *J. Non-Cryst. Solids*, **358** [3] 674–9 (2012).
- J. McCloy, N. Washton, P. Gassman, J. Marcial, J. Weaver, and R. Kukkadapu, "Nepheline Crystallization in Boron-Rich Alumino-Silicate Glasses as Investigated by Multi-Nuclear NMR, Raman, & Mössbauer Spectroscopies," *J. Non-Cryst. Solids*, **409**, 149–65 (2015).
- C. M. Jantzen and K. G. Brown, "Predicting the Spinel-Nepheline Liquidus for Application to Nuclear Waste Glass Processing. Part I: Primary Phase Analysis, Liquidus Measurement, and Quasicrystalline Approach," *J. Am. Ceram. Soc.*, **90**, 1866–79 (2007).
- C. M. Jantzen and K. G. Brown, "Predicting the Spinel-Nepheline Liquidus for Application to Nuclear Waste Glass Processing. Part II: Quasicrystalline Freezing Point Depression Model," *J. Am. Ceram. Soc.*, **90**, 1880–91 (2007).
- P. Hrma, B. J. Riley, J. V. Crum, and J. Matyas, "The Effect of High-Level Waste Glass Composition on Spinel Liquidus Temperature," *J. Non-Cryst. Solids*, **384**, 32–40 (2014).
- J. Matyas, J. D. Vienna, A. Kimura, M. Schaible, and R. M. Tate, "Development of Crystal-Tolerant Waste Glasses"; pp. 41–50 in *Advances in Materials Science for Environmental and Nuclear Technology*, Vol. 222, Edited by K. M. Fox, E. Hoffman, N. Manjooan and G. Pickrell. John Wiley & Sons, Inc., Hoboken, NJ, 2010.
- J. S. McCloy, M. J. Schweiger, C. P. Rodriguez, and J. D. Vienna, "Nepheline Crystallization in Nuclear Waste Glasses: Progress Towards Acceptance of High-Alumina Formulations," *Int. J. Appl. Glass Sci.*, **2** [3] 201–14 (2011).
- D. S. Kim, D. K. Peeler, and P. Hrma, "Effect of Crystallization on the Chemical Durability of Simulated Nuclear Waste Glasses"; pp. 177–85 in *Environmental and Waste Management Technologies in the Ceramic and Nuclear Industries (Ceram. Trans.)*, Vol. 61, Edited by V. Jain and R. Palmer. The American Ceramic Society, Westerville, OH, 1995.
- K. M. Fox, T. B. Edwards, and D. K. Peeler, "Control of Nepheline Crystallization in Nuclear Waste Glass," *Int. J. Appl. Ceram. Technol.*, **5**, 666–73 (2008).
- H. Li, J. D. Vienna, P. Hrma, D. E. Smith, and M. J. Schweiger, "Nepheline Precipitation in High-Level Waste Glasses: Compositional Effects and Impact on the Waste Form Acceptability"; pp. 261–8 in *Symposium on Scientific Basis for Nuclear Waste Management, MRS Proceedings*, Vol. 465, Cambridge University Press, New York, NY, 1996.
- J. S. McCloy and J. D. Vienna, "Glass Composition Constraint Recommendations for use in Life-Cycle Mission Modeling," PNNL-19372, 2010.
- J. D. Vienna, "Nuclear Waste Vitrification in the United States: Recent Developments and Future Options," *Int. J. Appl. Glass Sci.*, **1**, 309–21 (2010).
- D. K. Bailey and J. F. Schairer, "The System Na₂O–Al₂O₃–Fe₂O₃–SiO₂ at 1 Atmosphere, and the Petrogenesis of Alkaline Rocks," *J. Petrol.*, **7**, 114–70 (1966).
- J. L. Weaver, N. A. Wall, and J. S. McCloy, "Wet Chemical and UV-Vis Spectrometric Iron Speciation in Quenched Low and Intermediate Level Nuclear Waste Glasses," *MRS Online Proc. Libr.*, **1744**, 93–100 (2015).
- P. K. J. Deepika, K. S. Rathore, and N. S. Saxena, "Structural Characterization and Phase Transformation Kinetics of Se_{0.8}Ge_{4–x}Pb_x (x = 9, 12) Chalco-genide Glasses," *J. Non-Cryst. Solids*, **355** [22–23] 1274–80 (2009).
- M. Celikbilek, A. E. Ersundu, N. Solak, and S. Aydin, "Crystallization Kinetics of the Tungsten–Tellurite Glasses," *J. Non-Cryst. Solids*, **357** [1] 88–95 (2011).
- K. Matusita and S. Sakka, "Kinetic Study on non-Isothermal Crystallization of Glass by Thermal Analysis," *Bull. Inst. Chem. Res. Kyoto Univ.*, **59**, 159–71 (1981).
- N. Afify, M. A. Abdel-Rahim, A. S. Abd El-Halim, and M. M. Hafiz, "Kinetics Study of non-Isothermal Crystallization in Se_{0.7}Ge_{0.2}Sb_{0.1} Chalco-genide Glass," *J. Non-Cryst. Solids*, **128** [3] 269–78 (1991).
- A. Herrera-Gomez, *The Peak-Shirley Background*. Centro de Investigación y de Estudios Avanzados del Instituto Politécnico Nacional (CINVESTAV-IPN), Mexico, 2012.
- T. Yamashita and P. Hayes, "Analysis of XPS Spectra of Fe²⁺ and Fe³⁺ Ions in Oxide Materials," *Appl. Surf. Sci.*, **254** [8] 2441–9 (2008).
- W. G. Tasker, "X-ray Photoelectron Spectroscopy of Silicate Glasses"; Ph.D., Materials Science and Engineering, Massachusetts Institute of Technology, Boston, MA, 1987.
- P. I. K. Onorato, M. N. Alexander, C. W. Struck, G. W. Tasker, and D. R. Uhlmann, "Bridging and Nonbridging Oxygen Atoms in Alkali Aluminosilicate Glasses," *J. Am. Ceram. Soc.*, **68**, C-148–50 (1985).
- G. W. Tasker, D. R. Uhlmann, P. I. K. Onorato, M. N. Alexander, and C. W. Struck, "Structure of Sodium Aluminosilicate Glasses: X-ray Photoelectron Spectroscopy," *Le Journal de Physique Colloques*, **46**, C8–273 (1985).
- R. D. Shannon and T. Berzins, "Ionic Conductivity in low Carnegieite Compositions Based on NaAlSiO₄," *Mater. Res. Bull.*, **14**, 361–7 (1979).
- I. W. Donald, "Crystallization Kinetics of a Lithium Zinc Silicate Glass Studied by DTA and DSC," *J. Non-Cryst. Solids*, **345**, 120–6 (2004).
- M. Celikbilek, A. E. Ersundu, and S. Aydin, "Crystallization Kinetics of Amorphous Materials"; in *Advances in Crystallization Processes*, Edited by Y. Mastai. InTech, Rijeka, Croatia, 2012.
- J. F. Stebbins and Z. Xu, "NMR Evidence for Excess non-Bridging Oxygen in an Aluminosilicate Glass," *Nature*, **390**, 60–2 (1997).
- M. J. Toplis, S. C. Kohn, M. E. Smith, and I. J. F. Poplett, "Fivefold-Coordinated Aluminum in Tectosilicate Glasses Observed by Triple Quantum MAS NMR," *Am. Mineral.*, **85**, 1556–60 (2000).
- B. Mysen and P. Richet, *Silicate Glasses and Melts: Properties and Structure*, Vol. 10. Elsevier, Amsterdam, the Netherlands, 2005.
- P. Richet and Y. Bottinga, "Glass Transitions and Thermodynamic Properties of Amorphous SiO₂, NaAlSi₃O₈ and KAlSi₃O₈," *Geochim. Cosmochim. Acta*, **48**, 453–70 (1984).
- P. M. Sorensen, M. Pind, Y. Z. Yue, R. D. Rawlings, A. R. Boccaccini, and E. R. Nielsen, "Effect of the Redox State and Concentration of Iron on the Crystallization Behavior of Iron-Rich Aluminosilicate Glasses," *J. Non-Cryst. Solids*, **351**, 1246–53 (2005).
- M. Jensen, L. Zhang, and Y. Yue, "Probing Iron Redox State in Multi-component Glasses by XPS," *Chem. Geol.*, **322**, 145–50 (2012).
- K. H. Sun and M. L. Huggins, "Energy Additivity in Oxygen-Containing Crystals and Glasses," *J. Physical Chemistry*, **51**, 438–43 (1947).
- E. D. Zanotto, "Isothermal and Adiabatic Nucleation in Glass," *J. Non-Cryst. Solids*, **89**, 361–70 (1987).
- V. M. Fokin, M. L. F. Nascimento, and E. D. Zanotto, "Correlation Between Maximum Crystal Growth Rate and Glass Transition Temperature of Silicate Glasses," *J. Non-Cryst. Solids*, **351**, 789–94 (2005).
- P. F. James, "Kinetics of Crystal Nucleation in Silicate Glasses," *J. Non-Cryst. Solids*, **73**, 517–40 (1985).
- W. Holand and G. H. Beall, "Chapter 2: Composition Systems for Glass-Ceramics"; in *Glass-Ceramic Technology*, 2nd edition. John Wiley & Sons, Inc., Hoboken, NJ, 2012.
- L. C. Klein, B. V. Fasano, and J. M. Wu, "Viscous Flow Behavior of Four Iron-Containing Silicates With Alumina, Effects of Composition and Oxidation Condition," *J. Geophys. Res.: Solid Earth*, **88**, A880–6 (1983).
- D. A. Duke, J. F. MacDowell, and B. R. Karstetter, "Crystallization and Chemical Strengthening of Nepheline Glass-Ceramics," *J. Am. Ceram. Soc.*, **50**, 67–74 (1967).
- J. G. Thompson, R. L. Withers, A. K. Whittaker, R. M. Traill, and J. D. Fitzgerald, "A Reinvestigation of low-Carnegieite by XRD, NMR, and TEM," *J. Solid State Chem.*, **104**, 59–73 (1993).
- K. Onuma, T. Iwai, and K. Yagi, "Nepheline–Iron Nepheline' Solid Solutions," *J. Fac. Sci. Hokkaido University. Series 4, Geology and Mineralogy*, **15** [1–2] 179–90 (1972).
- A. A. Kruger, C. P. Rodriguez, J. B. Lang, A. R. Huckleberry, J. Matyas, and A. Owen, *Crystal-Tolerant Glass Approach for Mitigation of Crystal Accumulation in Continuous Melters Processing Radioactive Waste*. U.S. Department of Energy, Office of River Protection, Richland, WA, 2012.
- H. Li, P. Hrma, J. D. Vienna, M. Qian, Y. Su, and D. E. Smith, "Effects of Al₂O₃, B₂O₃, Na₂O, and SiO₂ on Nepheline Formation in Borosilicate Glasses: Chemical and Physical Correlations," *J. Non-Cryst. Solids*, **331**, 202–16 (2003).
- J. D. Vienna, et al., *Hanford Immobilized LAW Product Acceptance Testing: Tanks Focus Area Results (PNNL-13744)*. Pacific Northwest National Laboratory, Richland, WA, 2001.
- J. Marcial, J. Crum, O. Neill, and J. S. McCloy, "Nepheline Structural and Chemical Dependence on Melt Composition," *Am. Mineral.*, **101**, 266–76 (2016). □